EXAFS Studies of Uteroferrin and Its Anion Complexes

Anne E. True,[†] Robert C. Scarrow,[‡] Clayton R. Randall,[†] Richard C. Holz,[†] and Lawrence Que, Jr.*[,†]

Contribution from the Departments of Chemistry, University of Minnesota, Minneapolis, Minnesota 55455, and Haverford College, Haverford, Pennsylvania 19041

Received April 6, 1992

Abstract: Iron K-edge X-ray absorption data on the purple acid phosphatase from porcine uterus (uteroferrin, Uf) have been obtained for the native reduced enzyme and for the oxidized enzyme in its phosphate- and arsenate-bound forms. In all three complexes, the first sphere consists of 1.5 N/O at ~1.94 Å, 4 N/O at ~2.1 Å, and 0.5–1 N/O at ~2.4 Å; in no complex is found an Fe–O bond of ~1.8 Å which would derive from a μ-oxo bond. The ~1.94-Å shell corresponds to Fe–OAr and Fe–μ-OH(or R) bonds. The ~2.1-Å shell arises from histidine, carboxylate, oxoanion, and solvent ligation. The scatterer at ~2.4 Å is associated with a chelated carboxylate residue. The second-sphere analysis for Uf_r indicates an Fe–Fe distance of 3.52 Å, similar to those found for semimethemerythrin azide, methane monooxygenase, and related model complexes, which suggests the presence of a (μ-hydroxo or alkoxo)diiron unit supported by a carboxylate bridge. On the basis of the EXAFS analysis and other spectroscopic data, it is proposed that tyrosine and histidine are terminal ligands to the Fe(III) center, and histidine and the chelated carboxylate coordinate to the Fe(II) center, with solvent molecules completing the diiron coordination sphere. This proposed active site is slightly modified from that found for the R2 protein of ribonucleotide reductase from *Escherichia coli* and suggested for the hydroxylase component of methane monooxygenase. The diiron cores of $Uf_o{\cdot}PO_4$ and $Uf_o{\cdot}AsO_4$ are significantly different from that of Uf_r. Given the absence of a 1.8-Å bond, the diferric sites are not oxo-bridged, a conclusion also corroborated by the small intensity of the 1s → 3d preedge features in these complexes. The Fe–Fe distances of ~3.2–3.3 Å found for $Uf_o{\cdot}PO_4$ and $Uf_o{\cdot}AsO_4$ must then arise from an $Fe_2(OR)_2$ core. The observed Fe–P (3.17 Å) and Fe–As (3.41 Å) distances correspond to Fe–O–P(As) angles indicative of a bidentate bridging oxoanion which supports the Fe_2O_2 core.

The purple acid phosphatases (PAPs) are dinuclear iron enzymes (MW 35–40 kDa) that catalyze the in vitro hydrolysis of phosphate esters (including nucleoside triphosphates) under acidic pH conditions.[1,2] Though their in vivo function has not been established, it has been speculated that these enzymes may be involved in various cell regulation mechanisms.[1c,3] Best studied of the PAPs are the enzymes from porcine uterus (also called uteroferrin, Uf)[4] and bovine spleen (BSPAP).[5] The diiron active site can be found in two oxidation states: an enzymatically active Fe(III)Fe(II) form (PAP_r) which exhibits a pink color (λ_{max} = 510 nm, ϵ_M = 4000) and a rhombic EPR signal ($g_{av} \sim 1.75$), and an inactive (or considerably less active[6]) Fe(III)Fe(III) form (PAP_o) which is purple in color (λ_{max} = 560 nm, ϵ_M = 4000) and EPR silent. The distinctive chromophore of the PAPs arises from a tyrosine-to-Fe(III) charge-transfer transition, as demonstrated by resonance Raman spectroscopy.[5,7] The EPR, Mössbauer, and magnetic properties of the two forms indicate that the iron centers are antiferromagnetically coupled in both oxidation states.[4c,5,8–10] The PAPs thus belong to a class of diiron proteins[1b] which includes hemerythrin (Hr),[11] methane monooxygenase (MMO),[12] and the R2 protein of ribonucleotide reductase (RNR).[13]

The accumulated spectroscopic evidence suggests a (μ-hydroxo or alkoxo)diiron(II,III) active site for PAP_r,[5,8,9,14] similar to what is proposed for the mixed-valence forms of Hr,[15,16] with a single tyrosine bound to the Fe(III) center and one histidine ligand on each iron.[17] ESEEM[18] and electrochemical[19] data have indicated the presence of coordinated water, while a recent NOESY study

[†] University of Minnesota.
[‡] Haverford College.

(1) (a) Doi, K.; Antanaitis, B. C.; Aisen, P. *Struct. Bonding (Berlin)* **1988**, *70*, 1–26. (b) Que, L., Jr.; True, A. E. *Prog. Inorg. Chem.* **1990**, *38*, 97–200. (c) Vincent, J. B.; Averill, B. A. *FASEB J.* **1990**, *4*, 3009–3014.

(2) Abbreviations used: acac = acetylacetonato; BIPhMe = 2,2′-bis(1-methylimidazolyl)phenylmethoxymethane; BPMP-H = 2,6-bis[bis(2-pyridylmethyl)aminomethyl]-4-methylphenol; bpy = 2,2′-bipyridine; BSPAP = beef spleen purple acid phosphatase; $catH_2$ = catechol; $dipicH_2$ = pyridine-2,6-dicarboxylic acid; $ehgsH_3$ = *N*,*N*′-ethylene(*o*-hydroxyphenylglycine)salicylideneamine; ESEEM = electron spin echo envelope modulation; EXAFS = extended X-ray absorption fine structure; HDP-H = *N*-(*o*-hydroxybenzyl)-*N*,*N*-bis(2-pyridylmethyl)amine; HPTB-H = 1,3-bis[*N*,*N*-bis(2-benzimidazolylmethyl)amino]-2-hydroxypropane; Hr = hemerythrin; LMCT = ligand-to-metal charge transfer; Me_3TACN = 1,4,7-trimethyl-1,4,7-triazacyclononane; MMO = methane monooxygenase; OAc = acetate; OBz = benzoate; pz = pyrazole; RNR = ribonucleotide reductase; $salenH_2$ = *N*,*N*′-ethylenebis(salicylideneamine); TPA = tris(2-pyridylmethyl)amine; Uf = uteroferrin; XANES = X-ray absorption near-edge structure.

(3) Schindelmeister, J.; Münstermann, D.; Witzel, H. *Histochemistry* **1987**, *87*, 13–19.

(4) (a) Schlosnagle, D. C.; Bazer, F. W.; Tsibris, J. C. M.; Roberts, R. M. *J. Biol. Chem.* **1974**, *249*, 7574–7579. (b) Campbell, H. D.; Dionysius, A.; Keough, D. T.; Wilson, B. E.; de Jersey, J.; Zerner, B. *Biochem. Biophys. Res. Commun.* **1978**, *82*, 615–620. (c) Antanaitis, B. C.; Aisen, P.; Lilienthal, H. R. *J. Biol. Chem.* **1983**, *258*, 3166–3172.

(5) Averill, B. A.; Davis, J. C.; Burman, S.; Zirino, T.; Sanders-Loehr, J.; Loehr, T. M.; Sage, J. T.; Debrunner, P. G. *J. Am. Chem. Soc.* **1987**, *109*, 3760–3767.

(6) Dietrich, M.; Münstermann, D.; Suerbaum, H.; Witzel, H. *Eur. J. Biochem.* **1991**, *199*, 105–113.

(7) (a) Gaber, B. P.; Sheridan, J. P.; Bazer, F. W.; Roberts, R. M. *J. Biol. Chem.* **1979**, *254*, 8340–8342. (b) Antanaitis, B. C.; Strekas, T.; Aisen, P. *J. Biol. Chem.* **1982**, *257*, 3766–3770.

(8) Debrunner, P. G.; Hendrich, M. P.; de Jersey, J.; Keough, D. T.; Sage, J. T.; Zerner, B. *Biochim. Biophys. Acta* **1983**, *745*, 103–106.

(9) Day, E. P.; David, S. S.; Peterson, J.; Dunham, W. R.; Bonvoisin, J. J.; Sands, R. H.; Que, L., Jr. *J. Biol. Chem.* **1988**, *263*, 15561–15567.

(10) Sinn, E.; O'Connor, C. J.; de Jersey, J.; Zerner, B. *Inorg. Chim. Acta* **1983**, *78*, L13–L15.

(11) (a) Stenkamp, R. E.; Sieker, L. C.; Jensen, L. H. *J. Am. Chem. Soc.* **1984**, *106*, 618–622. (b) Sheriff, S.; Hendrickson, W. A.; Smith, J. L. *J. Mol. Biol.* **1987**, *197*, 273–296.

(12) Fox, B. G.; Froland, W. A.; Dege, J. E.; Lipscomb, J. D. *J. Biol. Chem.* **1989**, *264*, 10023–10033.

(13) Nordlund, P.; Sjöberg, B.-M.; Eklund, H. *Nature (London)* **1990**, *345*, 593–598.

(14) Pyrz, J. W.; Sage, J. T.; Debrunner, P. G.; Que, L., Jr. *J. Biol. Chem.* **1986**, *261*, 11015–11020.

(15) McCormick, J. M.; Reem, R. C.; Solomon, E. I. *J. Am. Chem. Soc.* **1991**, *113*, 9066–9079.

(16) Scarrow, R. C.; Maroney, M. J.; Palmer, S. M.; Que, L., Jr.; Roe, A. L.; Salowe, S. P.; Stubbe, J. *J. Am. Chem. Soc.* **1987**, *109*, 7857–7864.

(17) (a) Scarrow, R. C.; Pyrz, J. W.; Que, L., Jr. *J. Am. Chem. Soc.* **1990**, *112*, 657–665. (b) Wang, Z.; Ming, L.-J.; Que, L., Jr.; Vincent, J. B.; Crowder, M.; Averill, B. A. *Biochemistry* **1992**, *31*, 5263–5268. (c) Holz, R. C.; Que, L., Jr.; Ming, L.-J. *J. Am. Chem. Soc.* **1992**, *114*, 4434–4436.

0002-7863/93/1515-4246$04.00/0

of Fe(III)Co(II)Uf has identified a carboxylate bound to the Co(II) center.[17c] Phosphate and arsenate act as competitive inhibitors of enzyme activity and alter the spectroscopic and magnetic properties of the diiron core.[14,20-23] Furthermore, they potentiate the oxidation of the diiron center,[14,20] affording PAP_o complexes wherein the anion is tightly bound.[24]

The nature of the bridge in PAP_o is controversial. An oxo bridge as found in the crystallographically characterized diferric forms of Hr and RNR R2[11,13] was favored by early magnetic susceptibility studies;[10,20] so little paramagnetic susceptibility was detected for the phosphate complex of the oxidized PAP from bovine spleen ($BSPAP_o$·PO_4) that $-J$ was estimated to be >150 cm^{-1}.[5] However, neither resonance Raman[5] nor EXAFS spectroscopy[25,26] has found evidence for an Fe–O–Fe moiety in either Uf_o or $BSPAP_o$. More recent magnetic susceptibility studies on $BSPAP_o$·PO_4 suggest that the amount of coupling may be an order of magnitude lower than that previously reported.[27] Furthermore, comparison of the reduction potential of Uf at pH 7.0 with those of Hr, RNR R2, and MMO suggests that Uf, like MMO, does not contain a μ-oxo bridge.[19]

In this paper, we report analyses of the Fe K-edge EXAFS data for Uf_r, Uf_o·PO_4, and Uf_o·AsO_4 and provide new insights into the structure of the diiron site. In analyzing the data, we have carefully examined the questions of whether there is a μ-oxo bond present in the oxidized forms of Uf and how the tetraoxo anion inhibitors interact with the diferric active site.

Experimental Section

Model Complexes. Model complexes were synthesized according to published procedures. These included $Fe(acac)_3$,[28] $[Fe_2O(OAc)_2\{HB(pz)_3\}_2]$,[29] $[Fe_2O(OBz)(HDP)_2]BPh_4$,[30] $[Fe_2O(OAc)(TPA)_2](ClO_4)_3$,[31] and $[Fe_2O\{O_2P(OPh)_2\}(TPA)_2](ClO_4)_3$.[31]

Preparation of Protein Samples. Uteroferrin was isolated and purified from the uteri of gilts treated with 1,3,5(10)-estratriene-3,17β-diol 17-valerate as previously described.[4,32] The sample of reduced uteroferrin was prepared in 100 mM pH 4.9 acetate buffer containing 200 mM NaCl. β-Mercaptoethanol (0.1 M) and catalytic amounts of $Fe(NH_4)_2(SO_4)_2$ were used to reduce traces of oxidized uteroferrin and were subsequently removed by passage through a Sephadex G-25 column. The protein used was judged pure by its optical spectrum ($A_{280}/A_{512} \approx 14$) and by its ability to hydrolyze 10 mM *p*-nitrophenyl phosphate at pH 4.9 (specific activity $\approx$ 350 units/mg).[33] The sample was diluted with glycerol (20% by volume) to prevent ice crystal formation, concentrated to 250 μL (4.5 mM protein), and then frozen in a gold-plated copper sample holder with liquid nitrogen.

Uf_o·PO_4 and Uf_o·AsO_4 samples were prepared by adding phosphate (to give 100 mM phosphate) or arsenate (to give 50 mM arsenate) to a dilute sample of Uf_r ($\sim$250 μM) in acetate buffer at pH 4.9. These samples were maintained in air for $\sim$3–4 weeks at 4 °C, during which time the λ_{max} red-shifted to 560 nm ($A_{280}/A_{512} \approx 14$). EPR spectra of each sample were recorded to verify the absence of Uf_r and to determine the amount of adventitiously bound Fe(III), which in each case was <3%. Final sample concentrations were 6 mM for Uf_o·PO_4 and 4.2 mM for Uf_o·AsO_4.

EXAFS Data Collection and Analysis. X-ray absorption spectra (XAS) were collected between 6.9 and 8.0 keV at stations C-2 and A-3 of the Cornell High Energy Synchrotron Source (CHESS) and at beamline X9A at the National Synchrotron Light Source (NSLS) at Brookhaven National Laboratories (BNL). The monochromator was calibrated using the 7113.0-eV 1s $\rightarrow$ 3d peak in the XAS spectrum of $[Et_4N][FeCl_4]$ (suspended in Duco cement).[16] The XAS data of the protein samples were obtained as frozen solutions at ca. 100 K, while the data from the model compounds were collected as suspensions of the microcrystalline solids in boron nitride at ambient temperature. A_{exp} (C_f/C_o) was determined from an incident (C_o) ionization detector and a final fluorescence (C_f) detector. A large solid-angle Lytle fluorescence detector was used with a Mn filter and Soller slits.[34] The edge inflections in the X-ray absorption spectra of the various samples were monitored to determine whether photoreduction may occur upon prolonged exposure to the X-ray beam. No change in inflection occurred with beam exposure time, indicating that the oxidation states of the iron atoms were not significantly changed during data collection.

The treatment of the raw EXAFS data to yield χ is discussed at length in several review articles.[35,36] Details of our data treatment procedure, including correction of fluorescence data for thickness effects and detector response, have been presented previously.[16] The refinements reported were on $k^3\chi$ data, and the function minimized was $R \equiv \{\sum k^6(\chi_c - \chi)^2/n\}^{1/2}$, where the sum is over n data points between 2.5 and 13 Å^{-1}.

Single-scattering EXAFS theory allows the total EXAFS spectrum to be described as the sum of shells of separately modeled atoms as shown in eq 1[37]

$$\chi_c = \sum_{\text{shells}} nA[f(k)k^{-1}r^{-2}e^{-2\sigma^2k^2}\sin(2kr + \alpha(k))] \qquad (1)$$

where n is the number of atoms in a shell, $k = [8\pi^2m_e(E - E_0 + \Delta E)/h^2]^{1/2}$, and σ is the Debye–Waller factor. The amplitude reduction factor (A) and the shell-specific edge shift (ΔE) are empirical parameters that partially compensate for imperfections in the theoretical amplitude and phase functions f and α.[38]

Our analysis procedure, a variation of FABM (fine adjustment based on models),[39] uses theoretical amplitude and phase functions calculated using a curved-wave formalism.[40] For each shell, crystallographically characterized model complexes such as $[Fe^{III}(acac)_3]$ are used to determine A and ΔE.[38] This leaves two parameters per shell (r and n or σ^2) to be refined instead of the four parameters refined using BFBT (best fit based on theory).[39]

Integration of the 1s $\rightarrow$ 3d Peak. The preedge peak areas were calculated by subtracting an arctangent function from the data and normalizing with respect to the edge jump height. The background function was determined by a least-squares fit of an arctangent together with a first-order polynomial to the data below the inflection point of the edge as previously described.[41] The area of the preedge peak after the background subtraction was obtained by integrating over a range of $\sim$8 eV. This range centered on the peak and any residual background function was interpolated over that range. The edge jump was determined by fitting first-order polynomials to the data as previously described.[41] The difference between these two lines at the inflection point of the edge was used as the normalization factor for the preedge peak area. For example, the Uf_o·PO_4 has a normalized preedge peak area of 7.7×10^{-2} eV, which is abbreviated as 7.7 units.[42]

(18) Doi, K.; McCracken, J.; Peisach, J.; Aisen, P. *J. Biol. Chem.* **1988**, *263*, 5757–5763.
(19) Wang, D. L.; Holz, R. C.; David, S. S.; Que, L., Jr.; Stankovich, M. T. *Biochemistry* **1991**, *30*, 8187–8194.
(20) Davis, J. C.; Averill, B. A. *Proc. Natl. Acad. Sci. U.S.A.* **1982**, *79*, 4623–4627.
(21) Antanaitis, B. C.; Aisen, P. *J. Biol. Chem.* **1985**, *260*, 751–756.
(22) David, S. S.; Que, L., Jr. *J. Am. Chem. Soc.* **1990**, *112*, 6455–6463.
(23) Vincent, J. B.; Crowder, M.; Averill, B. A. *Biochemistry* **1991**, *30*, 3025–3034.
(24) (a) Keough, D. T.; Beck, J. L.; de Jersey, J.; Zerner, B. *Biochem. Biophys. Res. Commun.* **1982**, *108*, 1643–1648. (b) Burman, S.; Davis, J. C.; Weber, M. J.; Averill, B. A. *Biochem. Biophys. Res. Commun.* **1986**, *136*, 490–497.
(25) Kauzlarich, S. M.; Teo, B. K.; Zirino, T.; Burman, S.; Davis, J. C.; Averill, B. A. *Inorg. Chem.* **1986**, *25*, 2781–2785.
(26) Que, L., Jr.; Scarrow, R. C. *ACS Symp. Ser.* **1988**, *372*, 152–178.
(27) Gehring, S.; Fleischhauer, P.; Haase, W.; Dietrich, M.; Witzel, H. *Biol. Chem. Hoppe-Seyler* **1990**, *371*, 786.
(28) Iball, J.; Morgan, C. H. *Acta Crystallogr.* **1967**, *23*, 239–244.
(29) Armstrong, W. H.; Spool, A.; Papaefthymiou, G. C.; Frankel, R. B.; Lippard, S. J. *J. Am. Chem. Soc.* **1984**, *106*, 3653–3667.
(30) Yan, S.; Que, L., Jr.; Taylor, L. F.; Anderson, O. P. *J. Am. Chem. Soc.* **1988**, *110*, 5222–5224.
(31) Norman, R. E.; Yan, S.; Que, L., Jr.; Sanders-Loehr, J.; Backes, G.; Ling, J.; Zhang, J. H.; O'Connor, C. J. *J. Am. Chem. Soc.* **1990**, *112*, 1554–1562.
(32) Basha, S. M. M.; Bazer, F. W.; Geisert, R. D.; Roberts, R. M. *J. Anim. Sci.* **1980**, *50*, 113–123.
(33) Keough, D. T.; Dionysius, D. A.; de Jersey, J.; Zerner, B. *Biochem. Biophys. Res. Commun.* **1980**, *94*, 600–605.
(34) Stern, E. A.; Heald, S. M. *Rev. Sci. Instrum.* **1979**, *50*, 1579–1582.
(35) Teo, B.-K. In *EXAFS Spectroscopy, Techniques and Applications*; Teo, B.-K., Joy, D. C., Eds.; Plenum; New York, 1981; pp 13–58.
(36) Scott, R. A. *Methods Enzymol.* **1985**, *11*, 414–459.
(37) Bunker, G. B.; Stern, E. A. *Phys. Rev. Lett.* **1984**, *52*, 1990–1993.
(38) Teo, B.-K.; Lee, P. A. *J. Am. Chem. Soc.* **1979**, *101*, 2815–2832.
(39) Teo, B.-K.; Antonio, M. R.; Averill, B. A. *J. Am. Chem. Soc.* **1983**, *105*, 3751–3762.
(40) McKale, A. G.; Veal, B. W.; Paulikas, A. P.; Chan, S.-K.; Knapp, G. S. *J. Am. Chem. Soc.* **1988**, *110*, 3763–3768.
(41) Roe, A. L.; Schneider, D. J.; Mayer, R. J.; Pyrz, J. W.; Widom, J.; Que, L., Jr. *J. Am. Chem. Soc.* **1984**, *106*, 1676–1681.

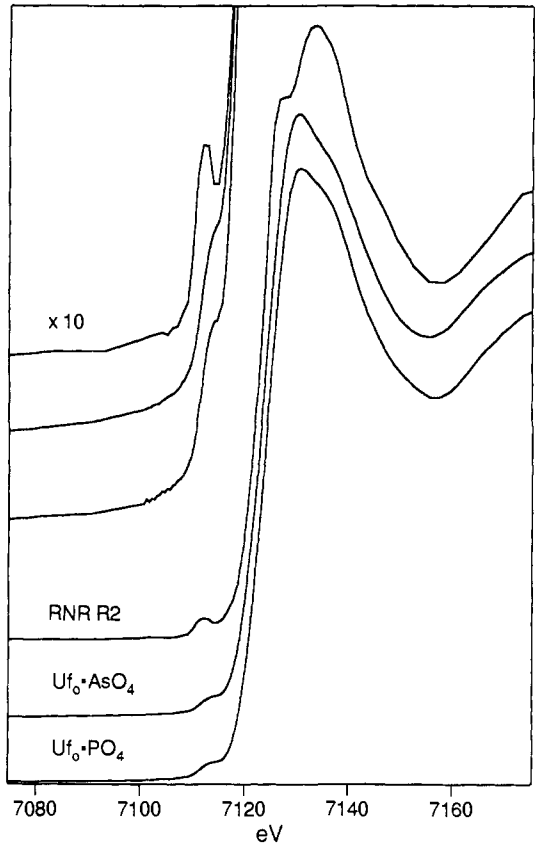

Figure 1. XANES spectra for RNR R2, Uf$_o$·AsO$_4$, and Uf$_o$·PO$_4$. The inset is a magnification of the 1s → 3d preedge transition and demonstrates the diminished intensity of the peak for the oxidized Uf samples when compared to the feature of a protein with a (μ-oxo)diferric center.

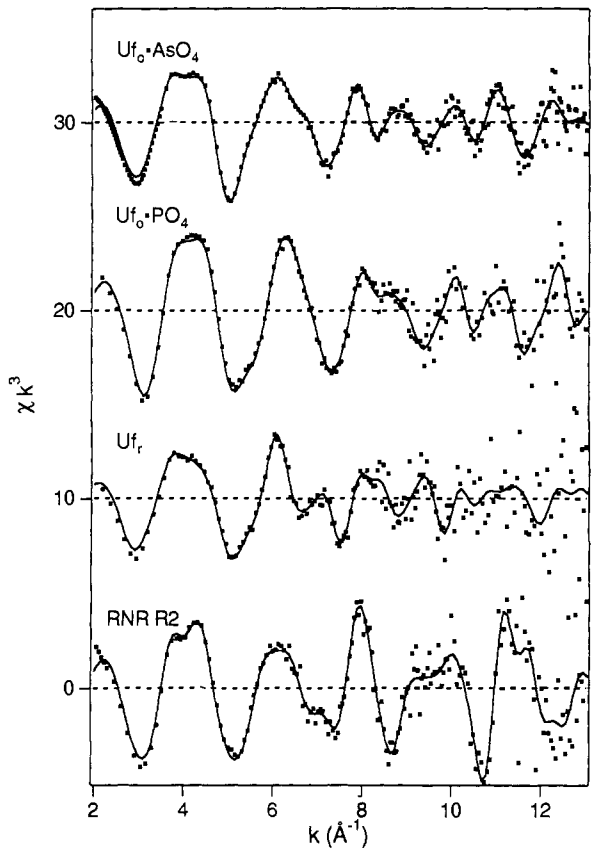

Figure 2. EXAFS spectra ($k^3\chi$) (■) obtained for Uf$_o$·AsO$_4$, Uf$_o$·PO$_4$, Uf$_r$, and native RNR R2, all obtained in fluorescence mode using frozen samples at ca. 100 K. The lines are smoothed data included only to aid visualization of the noisy data. The offsets between spectra correspond to $\Delta k^3\chi$ = 10 Å^{-3}.

Results and Discussion

Edge Region Analysis. Previous XANES studies and molecular orbital calculations on ferric model compounds have demonstrated that the intensity of the preedge 1s → 3d feature relative to the edge height jump can be correlated with the amount of iron 4p and 3d orbital mixing and, consequently, with the metal coordination environment.[41] In general, the amount of 4p and 3d orbital mixing and therefore the peak intensity decreases as the iron coordination environment changes from tetrahedral to octahedral, i.e. $I_{\text{tetrahedral}} > I_{\text{5-coordinate}} > I_{\text{octahedral}}$. However, 6-coordinate (μ-oxo)diiron complexes were found to have 1s → 3d peak areas larger than those of the corresponding mononuclear complexes, in a range indicative of a 5-coordinate mononuclear iron complex. This increase was attributed to the distortion of octahedral symmetry by the short μ-oxo bridge.[41]

The 1s → 3d preedge areas for the diferric Uf$_o$·PO$_4$ and Uf$_o$·AsO$_4$ are 6.8 and 7.4 units, respectively (Figure 1). These values are consistent with 6-coordinated monoferric or weakly coupled diferric complexes but lower than the values for 6-coordinate (μ-oxo)diiron(III) complexes,[41] metHrN$_3$, and RNR R2 (10.4 and 10.1 units, respectively). The mixed-valence Uf$_r$ has a preedge peak area of 4.8 units, comparable to the areas obtained for semimetHrN$_3$ (6.3 units) and [Fe$_2$(BPMP)(OPr)$_2$](BPh$_4$)$_2$ (4.7 units), both of which have 6-coordinate iron sites. Unfortunately, the preedge information is less useful for mixed-valence compounds because of the blurring of the XANES region by the differing edge energies of Fe(II) and Fe(III) and the lack of preedge data on structurally characterized synthetic Fe^{II}Fe^{III} compounds.

First-Sphere Analysis of the EXAFS Data. Figure 2 shows the raw and smoothed EXAFS data obtained for Uf$_r$, Uf$_o$·PO$_4$, and Uf$_o$·AsO$_4$, as well as our earlier reported data on the *Escherichia coli* RNR R2 protein[16] for comparison. The EXAFS oscillations become obscured by the noise at much lower k (wave vector) for the uteroferrin samples than for RNR R2. Though we at first thought that this was due to problems with our detection of the uteroferrin EXAFS, close inspection of the smoothed data of Uf in Figure 2 indicates that noise levels of Uf$_o$·PO$_4$, Uf$_o$·AsO$_4$, and RNR R2 are comparable.

Model Compounds. The first-sphere EXAFS analysis of the uteroferrin complexes is facilitated by considering the EXAFS spectra of the three model complexes, shown in Figure 3, which illustrate the effects of increasing the distribution of first-shell bond lengths. Fe(acac)$_3$ (Figure 3A) has six Fe–O bonds at virtually the same distance (1.99 Å by X-ray crystallography)[43] and gives a large-amplitude EXAFS spectrum close in shape to that predicted for a single Fe–O bond at one fixed distance. However, the μ-oxo-bridged complex [Fe$_2$O(OAc)$_2$(HBpz$_3$)$_2$] (Figure 3B) has an attenuated EXAFS spectrum due to destructive interference of the oscillations from the short Fe–O (1.78 Å) bond and from the longer Fe–O (average = 2.04 Å) and Fe–N (average = 2.16 Å) bonds.[29] The third model complex, [Fe$_2$O(OBz)(HDP)$_2$](BPh$_4$), has very little first-sphere EXAFS (Figure 3C). This can be explained by the destructive interference arising from the wide range of bond lengths in this complex (1.79, 1.93, 2.07, 2.17, and 2.27 Å).[30]

Table I shows the results of one-shell fits of the first-sphere Fourier-filtered EXAFS for three model compounds. As expected, single-shell fits were better for Fe(acac)$_3$ than for either of the other two model compounds which have a wider range of bond lengths. A problem with the single-shell fits shown in Table I for [Fe$_2$O(OAc)$_2$(HBpz$_3$)$_2$] and [Fe$_2$O(OBz)(HDP)$_2$](BPh$_4$)

(42) This unit has dimensions of electron volts × percent of edge height.

(43) Iball, J.; Morgan, C. H. *Acta Crystallogr.* **1967**, *23*, 239–244.

Table I. One- to Four-Shell Restricted Fits to the First-Sphere $k^3\chi$ EXAFS Data

	shell 1			shell 2			shell 3			shell 4			
fit	n	r	σ^2	n	r	σ^2	n	r	σ^2	n	r	σ^2	R (%)
						[Fe(acac)$_3$]							
A	6.0	2.00	0.003										13
B[a]	2.7	1.95	0.003	3.3	2.06	0.000							10
C	1.0	1.93	0.003	5.0	2.01	0.002							12
						[Fe$_2$O(OAc)$_2$(HBpz$_3$)$_2$]							
D	6.0	2.13	0.006										56
E[a]	1.0	1.78	0.003	5.0	2.13	0.004							19
F	1.0	1.78	0.003	4.0	2.10	0.003	1.0	2.22	0.003				17
						[Fe$_2$O(OBz)(HDP)$_2$](BPh$_4$)							
G	6.0	2.03	0.059										86
H	2.1	1.83	0.008	3.9	2.16	0.010							36
I[a]	1.0	1.81	0.003	5.0	2.14	0.023							22
J	1.0	1.81	0.003	4.0	2.07	0.035	1.0	2.19	0.003				24
K	1.0	1.79	0.003	1.0	1.91	0.003	3.0	2.14	0.006	1.0	2.30	0.003	26
L	1.0	1.79	0.003	1.0	1.90	0.003	1.0	2.07	0.003	3.0	2.21	0.010	22

[a] Two shell restricted fits with a shorter Fe–O and a longer Fe–N shell. In consideration of the expected coordination number of iron, $N_N + N_O = 6$.

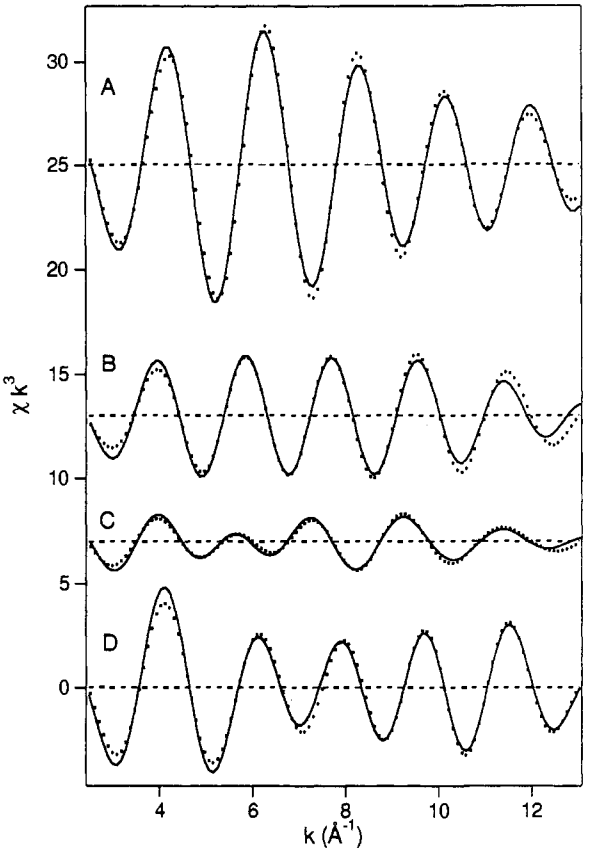

Figure 3. Comparison of the first-sphere Fourier-filtered (back-transformed 0.8–2.3 Å) $k^3\chi$ EXAFS spectra (■) of three model complexes and the R2 subunit of ribonucleotide reductase. The spectra shown are of (A) Fe(acac)$_3$, (B) [Fe$_2$O(OAc)$_2${HB(pz)$_3$}$_2$], (C) [Fe$_2$O(OBz)(HDP)$_2$](BPh$_4$), and (D) RNR R2. The simulations (—) shown in this figure correspond to fits A, F, and L in Table I. The simulation for RNR R2 is as described in ref 16.

is the large value of the Debye–Waller factors, which suggest that the first coordination sphere could be better modeled by two or more shells of atoms. The Debye–Waller factor of a particular shell reflects its vibrational disorder and the distribution of bond lengths represented by that shell. Based on the Fe(acac)$_3$ data, vibrational disorder at ambient temperature is adequately modeled with $\sigma^2 \approx 0.003$ Å^2; larger values indicate a shell containing a distribution of equilibrium bond lengths. In cases where $\sigma^2 > 0.01$ Å^2, one can generally find a statistically better fit employing multiple shells of scatterers.

Two-shell restricted fits are shown in Table I. As expected, addition of an auxiliary shell to the Fe(acac)$_3$ fit does not reduce the residual enough to justify the additional refined parameter (compare fits C and B to A, Table I). However, the fits with additional shells are significantly better (as judged by the residual) for the dinuclear complexes. For [Fe$_2$O(OAc)$_2$(HBpz$_3$)$_2$], the two-shell fit clearly indicates the presence of the 1.78 Å oxo bridge and five other ligands near 2.10 Å (Table I, fit E). Addition of a nitrogen shell reduces the residual further, although not enough to justify the additional refined parameter. We note, though, that the Fe–N bond length obtained (2.22 Å; fit F, Table 1) is quite close to the crystallographic bond length (2.19 Å) of the N trans to the oxo bridge.

The addition of a second shell to the fits for [Fe$_2$O(OBz)-(HDP)$_2$](BPh$_4$) decreases the residual (Table I, fits H and I) but still results in shells with large Debye–Waller factors (σ^2). For this complex, four shells are required to obtain a fit with a low residual and acceptable σ^2 values (Table I, fits K and L). It is difficult to choose between these two fits: K has σ^2 values that are more acceptable, while L has the lower residual. In fact, both models accurately describe the bond length distribution in the complex. The difference is that the principal shell for fit K contains the pyridyl nitrogens and the benzoate oxygen (average Fe–L distance 2.14 Å), while for fit L the primary shell contains all the nitrogens (2.20 Å average) but not the benzoate oxygen. Most of the refined distances are within 0.01–0.02 Å of the appropriately averaged crystallographic distances, the largest deviation being for the longest Fe–N distance in fit K (refined 2.30 Å; crystal 2.27 Å). We point out that both fits K and L recognize the presence of the short Fe-μ-oxo and the somewhat longer Fe–OPh bonds in separate shells.

First-Sphere Analysis of Uteroferrin. The first-sphere Fourier-filtered $k^3\chi$ EXAFS data of the uteroferrin complexes studied are shown in Figure 4; the low amplitudes of the EXAFS oscillations at higher k values suggest a diiron site with a wide range of bond lengths. The data for Uf$_r$ can be simulated with a single shell of 4–5 oxygen atoms at 2.06 Å (Fit A, Table II). However, the Debye–Waller factor is quite large ($\sigma^2 = 0.015$ Å^2) in comparison with that of Fe(acac)$_3$, suggesting a large spread of bond lengths in the first sphere. Furthermore, the single-shell fit does not reproduce the distinct interference pattern which appears at $k \approx 9$ Å^{-1}. Modeling the Fourier-filtered first-sphere data with two shells decreases σ^2 (Fits B and C; Table II), but the inclusion of a third shell at ~2.4 Å significantly reduces the residual and accurately reproduces the interference pattern at $k \approx 9$ Å^{-1} (Fits D and E, Table II).

The best fit for Uf$_r$ (Fit E, Table II, Figure 4) indicates a diiron site with scatterers at 1.93, 2.14, and 2.34 Å. We assign

Table II. One- to Three-Shell Restricted Fits to the Fourier-Filtered First-Sphere $k^3\chi$ Data of the Uf Samples[a]

	shell 1 (modeled as Fe–O)			shell 2 (modeled as Fe–N/O)			shell 3 (modeled as Fe–O)			
fit	n	r	σ^2	n	r	σ^2	n	r	σ^2	R (%)
					Uf_r[b]					
A	5.0	2.06	0.015							41
B	3.0	1.96	0.008	3.0	2.17	0.005				36
C	1.5	1.92	0.002	4.0	2.13	0.007				27
D	1.5	1.94	0.001	3.5	2.14	0.005	0.5	2.37	–0.002	11
E	1.5	1.93	0.001	3.5	2.14	0.004	1.0	2.34	0.004	11
					Uf_o·PO_4[c]					
F	5.0	2.04	0.014							20
G	3.0	1.97	0.009	3.0	2.13	0.011				24
H	1.5	1.94	0.004	3.5	2.09	0.008				15
I	1.5	1.94	0.004	3.5	2.10	0.009	0.5	2.45	0.004	10
J	1.5	1.94	0.003	3.5	2.10	0.008	1.0	2.44	0.011	8
					Uf_o·AsO_4[c]					
K	5.0	2.04	0.015							23
L	3.0	2.01	0.011	3.0	2.11	0.023				25
M	1.5	1.95	0.004	3.5	2.11	0.009				18
N	1.5	1.96	0.004	3.5	2.11	0.011	0.5	2.46	0.001	11
O	1.5	1.96	0.003	3.5	2.12	0.007	1.0	2.45	0.007	9

[a] Refinement and Fourier-transform range = 2.5–13.0 Å^{-1}. [b] Back-transform range = 0.9–2.3 Å. [c] Back-transform range = 0.8–2.3 Å.

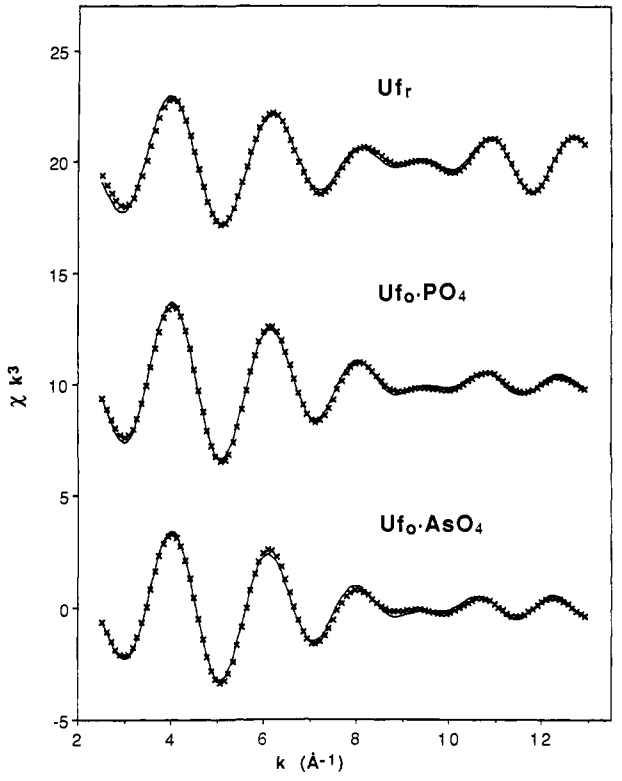

Figure 4. Comparison of the first-sphere Fourier-filtered (back-transformed 0.8–2.3 Å) $k^3\chi$ EXAFS spectra (×) of the three uteroferrin samples. The data shown are for Uf_r, Uf_o·PO_4, and Uf_o·AsO_4. The solid lines represent three-shell restricted fits (Table II; fits E, J, and O, respectively) to the data.

the 1.93-Å distance to Fe(III)–O(Tyr) and Fe(III)–μ-(OH or OR)Fe(II) bonds. Fe(III)–O(phenolate) bonds average about 1.90 Å,[44] and the presence of a tyrosine ligated to the Fe(III) center of Uf_r has been previously indicated by resonance Raman and NMR studies.[5,7,17] However, since there is only one Tyr per diiron unit, it would account for only 0.5 atom/Fe in the 1.93 Å shell. Lowest residuals were obtained with n = 1.5 for this shell (as shown in Table II), while σ^2 values refined to be negative when n was set to 0.5 or 1. A hydroxo or alkoxo bridge is an attractive candidate for the remaining O contribution in this shell, since it would afford the appropriate Fe–O bond distance and mediate the observed antiferromagnetic coupling between metal centers.[45,46]

The principal shell of 3.5 N/O at ~2.14 Å in Uf_r consists of a number of ligands with a range of bond lengths, as indicated by its somewhat larger Debye–Waller factor. Probable ligands with bond distances in this range include His (2.1–2.2 Å),[47] carboxylate (2.0–2.2 Å),[45a,b,47b–d,48] and solvent water (2.0–2.2 Å).[49] Clear evidence for the ligation of histidine and carboxylate residues comes from NMR studies,[17] while the presence of solvent in the metal coordination sphere is suggested by ESEEM and electrochemical studies.[18,19] It is also possible to divide the first coordination sphere into two shells with an equal number of scatterers as with $BSPAP_r$[25] (Fit B, Table II). However, the large Debye–Waller factors associated with both shells in such fits lead us to favor fits with a smaller number of scatterers in the ~1.95-Å shell and the remaining ligands in the ~2.1-Å shell.

The inclusion of a low Z atom at ~2.4 Å is required to accurately reproduce the interference pattern at $k \approx 9$ Å^{-1}. The only functional group among amino acid ligands likely to give rise to a scatterer at this distance is a carboxylate. In model complexes, such distances can be associated with either the carbon

(44) (a) Magurany, C. J.; Strouse, C. E. *Inorg. Chem.* **1982**, *21*, 2348–2350. (b) Lauffer, R. B.; Heistand, R. H., II; Que, L., Jr. *Inorg. Chem.* **1983**, *22*, 50–55. (c) Heistand, R. H., II; Roe, A. L.; Que, L., Jr. *Inorg. Chem.* **1982**, *21*, 676–681. (d) Davis, J. C.; Kung, W. S.; Averill, B. A. *Inorg. Chem.* **1986**, *25*, 394–396. (e) Pyrz, J. W.; Pan, X.; Que, L., Jr. *Inorg. Chem.* **1991**, *30*, 3462–3464.

(45) (a) Armstrong, W. H.; Lippard, S. J. *J. Am. Chem. Soc.* **1984**, *106*, 4632–4633. (b) Hartman, J. R.; Rardin, R. L.; Chaudhuri, P.; Pohl, K.; Wieghardt, K.; Nuber, B.; Weiss, J.; Papaefthymiou, G. C.; Frankel, R. B.; Lippard, S. J. *J. Am. Chem. Soc.* **1987**, *109*, 7387–7392. (c) Scheidt, W. R.; Cheng, B.; Safo, M. F.; Cukiernik, F.; Marchon, J.-C.; Debrunner, P. G. *J. Am. Chem. Soc.* **1992**, *114*, 4420–4421.

(46) (a) Ménage, S.; Que, L., Jr. *Inorg. Chem.* **1990**, *29*, 4293–4297. (b) Chen, Q.; Lynch, J. B.; Gomez-Romero, P.; Ben-Hussein, A.; Jameson, G. B.; O'Connor, C. J.; Que, L., Jr. *Inorg. Chem.* **1988**, *27*, 2673–2681. (c) Ménage, S.; Brennan, B. A.; Juarez-Garcia, C.; Münck, E.; Que, L., Jr. *J. Am. Chem. Soc.* **1990**, *112*, 6423–6425.

(47) (a) Gomez-Romero, P.; DeFotis, G. C.; Jameson, G. B. *J. Am. Chem. Soc.* **1986**, *108*, 851–853. (b) Gomez-Romero, P.; Casan-Pastor, N.; Ben-Hussein, A.; Jameson, G. B. *J. Am. Chem. Soc.* **1988**, *110*, 1988–1990. (c) Wu, F.-J.; Kurtz, D. M., Jr.; Hagen, K. S.; Nyman, P. D.; Debrunner, P. G.; Vankai, V. A. *Inorg. Chem.* **1990**, *29*, 5174–5183. (d) Tolman, W. B.; Liu, S.; Bentsen, J. G.; Lippard, S. J. *J. Am. Chem. Soc.* **1991**, *113*, 152–164. (e) Boinnard, D.; Cassoux, P.; Petroleas, V.; Savariault, J.-M.; Tuchauges, J.-P. *Inorg. Chem.* **1990**, *29*, 4114–4122.

(48) (a) Kitajima, N.; Fukui, H.; Moro-oka, Y. *J. Am. Chem. Soc.* **1990**, *112*, 6402–6403. (b) Ménage, S.; Zang, Y.; Hendrich, M. P.; Que, L., Jr. *J. Am. Chem. Soc.* **1992**, *114*, 7786–7792. (c) Hagen, K. S., personal communication. (d) Murch, B. P.; Bradley, F. C.; Que, L., Jr. *J. Am. Chem. Soc.* **1986**, *108*, 5027.

(49) (a) Murch, B. P.; Bradley, F. C.; Boyle, P. D.; Papaefthymiou, G. C.; Que, L., Jr. *J. Am. Chem. Soc.* **1987**, *109*, 7993–8003. (b) Murphy, T. B.; Johnson, D. K.; Rose, N. J.; Aruffo, A.; Schomaker, V. *Inorg. Chim. Acta* **1982**, *66*, L67–68.

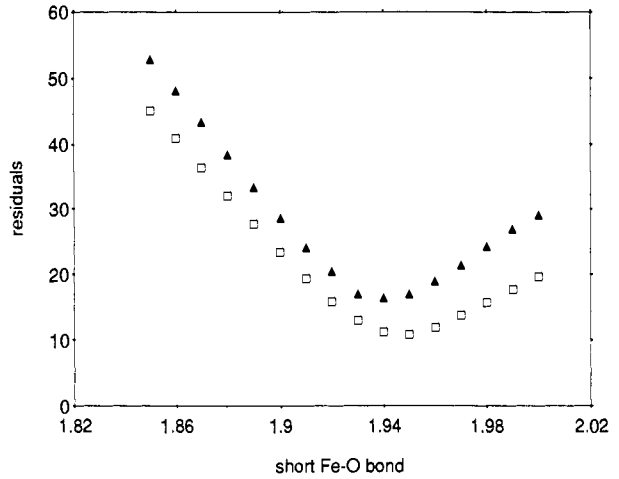

Figure 5. Plot of residual vs the shortest Fe–O bond length used in first-sphere fits for $Uf_o{\cdot}PO_4$ (▲) and $Uf_o{\cdot}AsO_4$ (□). For these fits, n, σ^2, and r for the short oxygen shell were held constant at 1 O/Fe, 0.003, and the indicated value, respectively, while the other shells were allowed to vary.

of a chelated carboxylate or the more weakly coordinated oxygen of an unsymmetrically chelated carboxylate but do not arise from the atoms of a bridging carboxylate.[45a,b,47b-d] In [Fe{HB(3,5-*i*-$Pr_2pz)_3$}(OBz)(CH_3CN)], the chelated benzoate has Fe–O bonds of 2.135(8) and 2.252(8) Å and an Fe–C(carboxylate) distance of 2.51 Å.[48a] In [Fe(cyclen)OAc](CF_3SO_3), the unsymmetrically chelated acetate has Fe–O bond lengths of 2.04 and 2.35 Å and an Fe–C(carboxylate) distance of 2.53 Å.[48c] An unsymmetrically chelated mode has also been assigned for the terephthalate carboxylate when bound to protocatechuate 3,4-dioxygenase.[50] Though we cannot distinguish between these two alternatives, the requirement for a low Z scatterer at ca. 2.4 Å in the fits implicates a chelated carboxylate ligand in the diiron site.

The first-sphere Fourier-filtered spectra for the oxidized complexes, $Uf_o{\cdot}PO_4$ and $Uf_o{\cdot}AsO_4$, have fits that are very similar to those of Uf_r. The one-shell fits reveal a similar average bond length with comparably large σ^2 values (Fits F and K, Table II); however, the best fits are derived from the inclusion of three shells at ca. 1.95, 2.10–2.11, and 2.45 Å (Fits I, J, N, and O, Table II), suggesting that the coordination environments of the iron centers have not changed significantly upon oxidation. The somewhat shorter principal shell for the oxidized complexes probably reflects their higher oxidation state and the presence of oxoanion in the coordination sphere. (The Fe–O bonds of coordinated oxoanions typically are shorter than the 2.1-Å average associated with the principal shell.[51,52])

There is no evidence for a μ-oxo bridge in the oxidized complexes. Figure 5 shows the effect of varying the length of the shortest Fe–O bond on the residual of the first-sphere fits for $Uf_o{\cdot}PO_4$ and $Uf_o{\cdot}AsO_4$. It is clear that the best fits arise from Fe–O bond lengths of ca. 1.94 Å, which are much too long for an Fe(III)–μ-oxo bond but expected for an Fe(III)–phenolate bond.[44] This distance is similar to that found in Uf_r, suggesting that this scatterer can indeed be attributed to the tyrosine on the redox-inactive ferric center. As with Uf_r, the other scatterer at ~1.95 Å is best assigned to the bridging ligand which mediates the antiferromagnetic coupling observed for the diiron center. The bond distance observed is most consistent with a bridging hydroxide[45] or alkoxide.[46]

In an earlier EXAFS study of BSPAP, Kauzlarich et al. similarly found no evidence for an Fe–O distance attributable to a μ-oxo bridge between the ferric centers.[25] It was suggested that the absence of a short Fe–μ-O bond was the result of interference due to the Fe–O(Tyr) bond at ca. 1.9 Å. As our analysis of $[Fe_2O(OBz)(HDP)_2](BPh_4)$ demonstrates (vide supra), both the Fe–μ-oxo and Fe–O(phenolate) distances can be discerned in an EXAFS spectrum when both are present. Furthermore, EXAFS analysis has previously established the presence of an Fe–μ-oxo bond in two related proteins, metHr and RNR R2.[16,53,54] *Thus, the analysis of our EXAFS data argues against the presence of an oxo bridge with the typical 1.8-Å bond length in oxidized PAPs.* The EXAFS analyses of the first coordination sphere of BSPAP in general agree with our results, though the bond distances found for Uf are slightly shorter. For example, in Table II, compare fit B with the 2-shell fit for $BSPAP_r$ (3 O/N each at 2.01 and 2.17 Å) and fit G with the 2-shell fit for $BSPAP_o{\cdot}PO_4$ (3 O/N each at 1.98 and 2.15 Å).

Second- and Third-Sphere EXAFS Analysis. Model Compounds. The magnitude of the Fe–Fe separation and the presence of oxoanions in the coordination sphere of the diiron site can, in principle, be determined from the analysis of the second-sphere EXAFS data of the uteroferrin complexes. For comparison, we obtained EXAFS data on $[Fe_2O(OAc)(TPA)_2](ClO_4)_3$ and $[Fe_2O\{O_2P(OPh)_2\}(TPA)_2](ClO_4)_3$, both of which have crystal structures.[31] Replacing the carbon atom of the carboxylate bridge with phosphorus clearly enhances the second-sphere peak in the Fourier-transformed data, indicating the introduction of a large Z scatterer in this region (Figure 6).

The EXAFS features of these complexes are well simulated with parameters similar to those determined by X-ray analysis. In addition to the first-shell scatterers (1 oxygen at 1.80 Å, 1 oxygen at 1.95–2.00 Å, and 4 nitrogens at ~2.16 Å), the diferric models have two shells each of 5–8 carbons at ~3.03 and ~4.35 Å, as well as Fe–Fe and Fe–oxoanion interactions at various distances. The Fe–Fe distances determined by EXAFS for the acetate and phosphate complexes are 3.24 and 3.38 Å, respectively, compared with 3.29 and 3.36 Å, respectively, from the X-ray analysis. The disparity between the EXAFS and crystallographic values may be attributed to correlations with Fe–C and Fe–Fe distances. However, the Fe–P distance of 3.20 Å determined by EXAFS matches the X-ray value of 3.21 Å.

Reduced Uteroferrin. A similar fitting procedure was used to determine the scattering shells present in the protein samples. To eliminate some of the noise in the data, the refinements were carried out on Fourier-filtered data, and the back-transform range (0.8–4.1 Å) included all of the peaks of interest. Results of the fitting procedure are summarized in Table III. For ease of comparison of the various complexes, we have chosen first-sphere fits with a principal shell of O/N atoms at ~2.1 Å and two auxiliary shells at ~1.95 and ~2.4 Å.

The Fourier transform of the filtered $k^3\chi$ EXAFS data for Uf_r is shown in Figure 7. The features at $r' \approx 3$ Å can be simulated with two shells at ca. 3.2 and 3.5 Å that are associated with either 1 Fe or a number of low Z scatterers. As discussed in detail by DeWitt et al. in their analysis of the EXAFS spectra of methane monooxygenase,[55] this ambiguity results from the comparable scattering properties of a single Fe atom and a combination of several low-Z atoms at the same distance, and there is a strong

(50) True, A. E.; Orville, A. M.; Pearce, L. L.; Lipscomb, J. D.; Que, L., Jr. *Biochemistry* **1990**, *29*, 10847–10854.

(51) (a) Drüeke, S.; Wieghardt, K.; Nuber, B.; Weiss, J.; Fleischhauer, H.-P.; Haase, W. *J. Am. Chem. Soc.* **1989**, *111*, 8622–8631. (b) Turowski, P. N.; Armstrong, W. H.; Roth, M. E.; Lippard, S. J. *J. Am. Chem. Soc.* **1990**, *112*, 681–690. (c) Schepers, K.; Bremer, B.; Krebs, B.; Henkel, G.; Althaus, E.; Mosel, B.; Müller-Warmuth, W. *Angew. Chem., Intl. Ed. Engl.* **1990**, *29*, 531–533. (d) Bremer, B.; Schepers, K.; Fleischhauer, P.; Haase, W.; Henkel, G.; Krebs, B. *J. Chem. Soc., Chem. Commun.* **1991**, 510–511.

(52) (a) Jang, H. G.; Hendrich, M. P.; Que, L., Jr. *Inorg. Chem.* **1993**, *32*, 911. (b) Jang, H. G.; Que, L., Jr., unpublished observations.

(53) (a) Zhang, K.; Stern, E. A.; Ellis, F.; Sanders-Loehr, J.; Shiemke, A. K. *Biochemistry* **1988**, *27*, 7470–7479. (b) Elam, W. T.; Stern, E. A.; McCallum, J. D.; Sanders-Loehr, J. *J. Am. Chem. Soc.* **1982**, *104*, 6369–6373.

(54) Bunker, G.; Petersson, L.; Sjöberg, B.-M.; Sahlin, M.; Chance, M.; Chance, B. *Biochemistry* **1987**, *26*, 4708–4716.

(55) DeWitt, J. G.; Bentsen, J. G.; Rosenzweig, A. C.; Hedman, B.; Green, J.; Pilkington, S.; Papaefthymiou, G. C.; Dalton, H.; Hodgson, K. O.; Lippard, S. J. *J. Am. Chem. Soc.* **1991**, *113*, 9219–9235.

Table III. Restricted Multishell Fits to the Outer-Sphere $k^3\chi$ EXAFS Data of the Uf Samples[a]

	Fe–C			Fe–Fe			Fe–P/As			Fe–C			
fit	n	r	σ^2	n	r	σ^2	n	r	σ^2	n	r	σ^2	R (%)
					Uf_r[b]								
A				1	3.53	0.008							38
B				1	3.15	0.007							28
C	1.5	3.54	0.001	1	3.16	0.007							25
D	3.2	3.20	0.002	1	3.52	0.011							21
E	1.5	3.54	0.001	1	3.16	0.007				4	4.31	0.005	20
F	3.2	3.20	0.001	1	3.52	0.012				3	4.31	0.002	13
					$Uf_o{\cdot}PO_4$[c]								
G				1	3.27	0.009							30
H				1	3.22	0.004	1	3.17	0.001				23
I				1	3.22	0.004	1	3.17	0.001	4.7	4.34	0.006	16
					$Uf_o{\cdot}AsO_4$[d]								
J				1	3.28	0.004							26
K				1	3.29	0.002	1	3.41	0.007				19
L				1	3.29	0.002	1	3.41	0.007	3.9	4.33	0.006	13

[a] The first-sphere parameters used to obtain the second- and third-sphere fits for Uf_r, $Uf_o{\cdot}PO_4$, and $Uf_o{\cdot}AsO_4$ in this table come from fits E, J, and O of Table II, respectively, and did not change significantly upon the addition of the outer-sphere shells. The refinement and Fourier-transform range used for all three samples was 2.5–13.0 Å^{-1}. [b] Back-transform range = 0.9–4.0 Å. [c] Back-transform range = 0.8–4.1 Å. [d] Back-transform range = 0.8–4.0 Å.

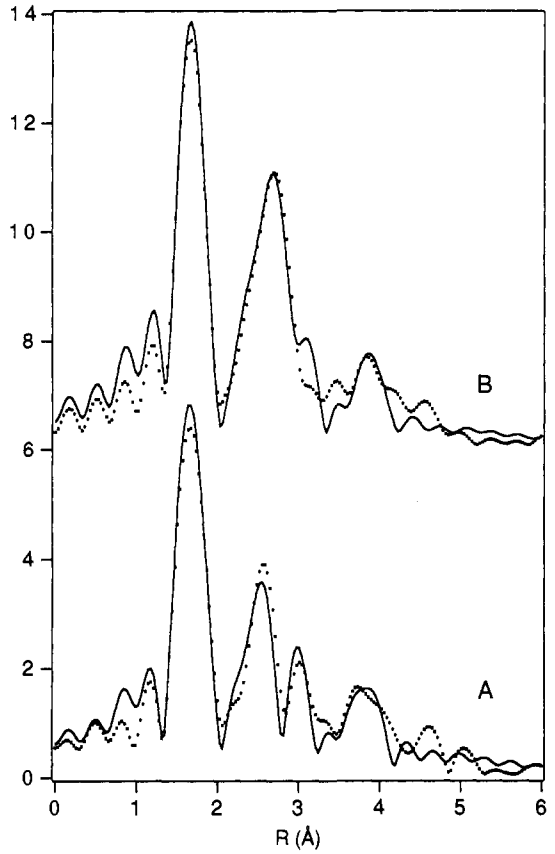

Figure 6. Experimental (■) Fourier-transformed (3.0–13.0 Å^{-1}) $k^3\chi$ data for (A) $[Fe_2O(OAc)(TPA)_2](ClO_4)_3$ and (B) $[Fe_2O\{O_2P(OPh)_2\}(TPA)_2](ClO_4)_3$. The parameters for the simulated data (—) are (A) 1 Fe–O at 1.79 Å, 1 Fe–O at 2.00 Å, 4 Fe–N at 2.17 Å, 8 Fe–C at 3.02 Å, 1 Fe–Fe at 3.24 Å, and 5 Fe–C at 4.34 Å; (B) 1 Fe–O at 1.79 Å, 1 Fe–O at 2.00 Å, 4 Fe–N at 2.17 Å, 5.4 Fe–C at 3.03 Å, 1 Fe–P at 3.20 Å, 1 Fe–Fe at 3.38 Å, and 4.5 Fe–C at 4.36 Å.

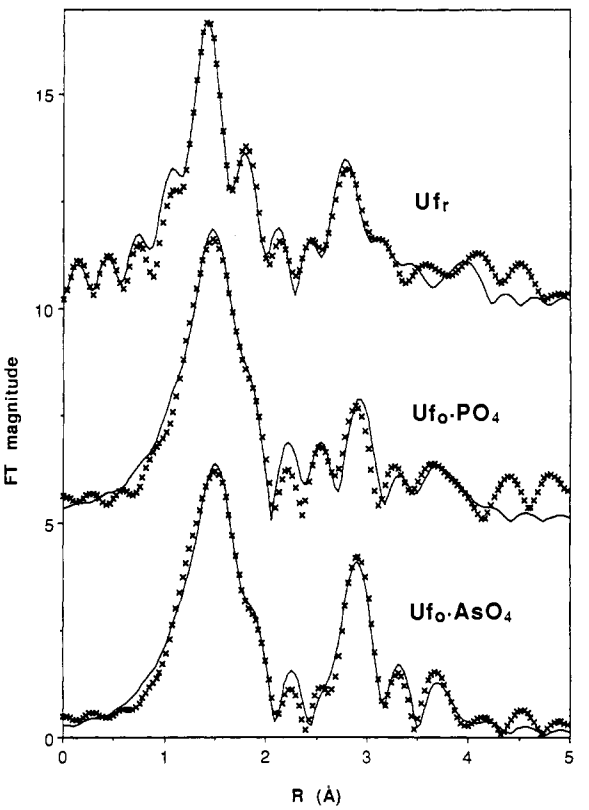

Figure 7. Observed (×) and calculated (—) $k^3\chi$ data Fourier-transformed between k = 2.5 and 13 Å^{-1} for Uf_r (Table III, fit F), $Uf_o{\cdot}PO_4$ (Table III, fit I), and $Uf_o{\cdot}AsO_4$ (Table III, fit L).

correlation between these two shells. For Uf_r, we can obtain fits with 1 Fe at 3.15 Å and 1.5 C at 3.54 Å or 1 Fe at 3.52 Å and 3.2 C at 3.20 Å. Note that the Fe–Fe distances obtained in the two fits differ by ca. 0.4 Å; similarly, the analysis for methane monooxygenase yielded two possible Fe–Fe distances that differed by ca. 0.4 Å.[55] We favor the fit with the longer Fe–Fe distance, because it reproduces the $r' \approx$ 3-Å features well and affords a better residual. Inclusion of low Z scatterers at 4.3 Å further decreases the residual. The low Z scatterers at 3.2 and 4.3 Å are associated with the outer-shell C and N atoms of coordinated imidazoles that have been identified by NMR.[17]

The 3.52 Å Fe–Fe distance suggests the presence of an $Fe_2(\mu\text{-OR})$ unit supported by bridging carboxylates as observed for other mixed valent diiron complexes such as semimethemerythrin azide (3.46 Å),[16] MMO hydroxylase in the mixed-valent state (average 3.42 Å),[55] and synthetic (μ-phenoxo)bis(μ-carboxylato)diiron(II,III) complexes (3.37, 3.43, and 3.49 Å).[56] While the R in an $Fe_2(\mu\text{-OR})$ unit can, in principle, be H, alkyl, or aryl,[45,46,56] a phenolate bridge can be eliminated on the basis of NMR and UV–vis spectral arguments. A hydroxo or alkoxo bridge is consistent with the weak antiferromagnetic coupling found for

Uf_r[9] and would provide two of the three bonds at ~1.93 Å required by the first-shell EXAFS fit (with the third being the Fe(III)–O(Tyr) bond).

The presence of one or more carboxylate bridges is suggested by the 3.52-Å Fe–Fe distance. Without an additional bridge, the Fe–Fe scattering for a $Fe_2(\mu\text{-OR})$ unit would likely be motionally broadened to the point of being unobservable; for example, no second-sphere scattering is evident in the EXAFS spectrum of the singly bridged $[Cl_3Fe\text{-}O\text{-}FeCl_3]^{2-}$ complex.[57] Furthermore, it has been found in a series of (μ-alkoxo)diiron complexes that the Fe–Fe distance can be constrained from 3.7[51d] to ~3.5 Å[46b,c] by a bidentate carboxylate bridge. Bridging carboxylates have been a feature of several proposals for the PAP active site,[1c,17,23,25] mainly because of the established presence of such bridges in related proteins such as hemerythrin and ribonucleotide reductase.[11,13] However, there is currently no unequivocal evidence that requires their presence.

Oxidized Uteroferrin Anion Complexes. The Fourier transforms of the filtered $k^3\chi$ EXAFS data for $Uf_o{\cdot}PO_4$ and $Uf_o{\cdot}AsO_4$[58] are shown in Figure 7. The oxidized complexes have more intense features (relative to Uf_r) in the $r' = 3$ Å region of the Fourier-transformed EXAFS spectra which are best simulated by Fe and P or As scatterers. Probably because of the stronger scattering properties of the heavier atoms, carbon scatterers at 3.2 Å only improved the fits a little and were thus not included. However, the inclusion of carbon scatterers at 4.3 Å did significantly improve the residual; these scatterers correspond to features in the $r' =$ 3.8-Å region of the Fourier-transformed EXAFS spectra.

For $Uf_o{\cdot}PO_4$, a reasonable fit is obtained with an Fe–Fe distance of 3.21 Å and an Fe–P distance of 3.17 Å (Fits H and I, Table III; Figure 7). An alternative simulation with an Fe–Fe distance of 3.44 Å was eliminated because of its extremely high σ^2 value (>0.04 Å^2). We were unable to simulate our EXAFS data with an Fe–Fe distance near 3.01 Å and an Fe–P distance near 3.06 Å as reported by Kauzlarich et al. for $BSPAP_o{\cdot}PO_4$[25] and conclude that such distances are not present in $Uf_o{\cdot}PO_4$.

For $Uf_o{\cdot}AsO_4$, the second-shell data can best be modeled with an Fe–Fe distance of 3.29 Å and an Fe–As distance of 3.41 Å (Fits K and L, Table III; Figure 7). Attempts to fit the data with the assignments of the Fe–Fe and Fe–As distances reversed did not converge. Our results are supported by the following arguments: (1) the complex $[Fe_2(AsO_4)_3(Me_3TACN)_2]$ exhibits an average Fe–As distance of 3.43 Å,[51a] a value that matches well with our fits; and (2) $Uf_o{\cdot}PO_4$ and $Uf_o{\cdot}AsO_4$ are likely to be structurally related, and the shorter Fe–Fe distance agrees more closely with that determined for $Uf_o{\cdot}PO_4$ (3.21 Å).

The shorter Fe–Fe separation in the $Uf_o{\cdot}XO_4$ complexes relative to that of Uf_r implies a change in the structure of the diiron core. While the 3.2–3.3-Å distance observed is consistent with the presence of a (μ-oxo)diiron core additionally supported by bidentate oxoanion bridges,[31,51a,b] the short Fe–O bonds (1.8 Å) required by the μ-oxo bridge are clearly excluded by the intensities of the preedge features and the first-sphere analyses of $Uf_o{\cdot}PO_4$ and $Uf_o{\cdot}AsO_4$ (vide supra). Carboxylate-bridged diferric complexes having longer Fe–μ-O bonds consistent with the first-sphere analysis exhibit Fe–Fe distances that are at least 0.2 Å longer than the μ-oxo complexes (e.g., μ-hydroxo, $[Fe_2OH(OAc)_2\{HB(pz)_3\}_2]ClO_4$, 3.44 Å;[45a] μ-alkoxo, $[\{Fe_2(HPTB)OBz\}_2O_2](ClO_4)_2(OTs)_2$, 3.55 Å;[46b] μ-phenoxo, $Me_4N[Fe_2HXTA(OAc)_2]$, 3.442 Å[48d]). Corresponding complexes with phosphate bridges would be expected to have even longer Fe–Fe distances because of the larger bite of the phosphate; this principle is illustrated by the following comparisons: $[Fe_2O(OAc)_2\{HB(pz)_3\}_2]$ (3.15 Å)[29] vs $[Fe_2O\{O_2P(OPh)_2\}_2\{HB(pz)_3\}_2]$ (3.34 Å);[51b] $[Fe_2O(TPA)_2(OAc)](ClO_4)_3$ (3.24 Å) vs $[Fe_2O(TPA)_2\{O_2P(OPh)_2\}](ClO_4)_3$ (3.36 Å);[31] $[Fe_2BPMP(O_2CC_2H_5)_2]BPh_4$ (3.35 Å)[56a] vs $[Fe_2BPMP\{O_2P(OPh)_2\}_2]Cl$ (3.68 Å).[52a] Thus an $Fe_2(\mu\text{-OR})$ unit supported by bidentate XO_2 bridges would be inconsistent with the observed Fe–μ-O and Fe–Fe distances in $Uf_o{\cdot}PO_4$ and $Uf_o{\cdot}AsO_4$.

The observed Fe–μ-O and Fe–Fe distances in $Uf_o{\cdot}PO_4$ and $Uf_o{\cdot}AsO_4$ can be rationalized by the presence of an $Fe_2(\mu\text{-OR})_2$ core. This class of complexes has Fe–Fe distances that range from 3.1 to 3.3 Å,[46a,59] and the bridging oxygen atoms are typically bound unsymmetrically to the two iron centers with Fe–μ-O bonds that are ca. 1.9 Å to one Fe and 2.1 Å to the other, thus affording two of the three short (1.9 Å) bonds found in the first-sphere analysis (the third being the Fe–O(Tyr) bond).

From the EXAFS analysis, the oxoanion is clearly coordinated to the diiron core; however, there are several possible coordination modes to consider, such as monodentate or bidentate, terminal or bridging. Since chemical analysis of $PAP_o{\cdot}PO_4$ complexes indicates that one phosphate is bound per mole of enzyme,[24] the number (i.e., 0.5 or 1) of P or As scatterers found per Fe can, in principle, ascertain whether the oxoanion is bound to one or both iron centers in uteroferrin. However, it is difficult to determine the number of scatterers in each shell precisely with EXAFS.

On the other hand, the Fe–X distances determined are much more reliable. The Fe–X distances obtained, together with typical Fe–OX and X–O bond lengths, may be used to calculate the Fe–O–X angle and to deduce the coordination mode of the oxoanion. Table IV lists a number of structurally characterized metal–oxoanion complexes and their M–X distances and M–O–X angles. Monodentate oxoanion complexes have large M–O–X angles (>145°) due to the lack of constraints on the uncoordinated oxygen atoms. Bidentate anions bridging iron centers without a single atom bridge appear somewhat more constrained but still can give rise to similarly large angles. Bridging bidentate anions on an $Fe_2(\mu\text{-OR})$ unit are the most constrained and typically afford an M–O–X angle near 130°; this coordination mode is the most common among the synthetic complexes. While there are presently no structurally characterized iron complexes with chelated oxoanions, such a binding mode would be expected to afford relatively acute Fe–O–X angles (~90°).

On the basis of the Fe–X values deduced from the EXAFS fits, estimated Fe–O(XO_4) bond lengths of 2.0 Å, and P–O and As–O bond lengths of 1.5 and 1.7 Å, respectively, Fe–O–X angles of 129° and 134° can be calculated for $Uf_o{\cdot}PO_4$ and $Uf_o{\cdot}AsO_4$, respectively. These values exclude a terminal monodentate or chelated mode for the binding of these anions to uteroferrin. Our conclusions disagree with the earlier suggestion of Kauzlarich et al. that phosphate is bound in a terminal monodentate mode in $BSPAP_o{\cdot}PO_4$. On the basis of our calculations, their Fe–P distance

(56) (a) Borovik, A. S.; Papaefthymiou, V.; Taylor, L. F.; Anderson, O. P.; Que, L., Jr. *J. Am. Chem. Soc.* **1989**, *111*, 6183–6195. (b) Buchanan, R. M.; Mashuta, M. S.; Richardson, J. F.; Oberhausen, K. J.; Hendrickson, D. N.; Webb, R. J.; Nanny, M. A. *Inorg. Chem.* **1990**, *29*, 1299–1301. (c) Ben-Hussein, A.; Morris, N. L.; Gomez-Romero, P.; Jameson, G. B., unpublished results. (d) Suzuki, M.; Oshio, H.; Uehara, A.; Endo, K.; Yanaga, M.; Kida, S.; Saito, K. *Bull. Chem. Soc. Jpn.* **1988**, *61*, 3907–3913.

(57) Scarrow, R. C., unpublished observations.

(58) We have not investigated the EXAFS spectrum of Uf_o, because we have not been able to generate a spectroscopically homogeneous sample. Its Mössbauer spectrum indicates the presence of a number of different species; in contrast, the Mössbauer spectrum of $Uf_o{\cdot}PO_4$ exhibits a pair of quadrupole doublets of equal intensity, as expected for a homogeneous sample.

(59) (a) Thich, J. A.; Oh, C. C.; Powers, D.; Vasilou, B.; Mastropaolo, D.; Potenza, J. A.; Schugar, H. J. *J. Am. Chem. Soc.* **1976**, *98*, 1425–1433. (b) Borer, L.; Thalken, L.; Ceccarelli, C.; Glick, M.; Zhang, J. H.; Reiff, W. M. *Inorg. Chem.* **1983**, *22*, 1719–1724. (c) Chiari, B.; Piovesana, O.; Tarantelli, T.; Zanazzi, P. F. *Inorg. Chem.* **1982**, *21*, 2444. (d) Chiari, B.; Piovesana, O.; Tarantelli, T.; Zanazzi, P. F. *Inorg. Chem.* **1984**, *23*, 3398. (e) Chiari, B.; Piovesana, O.; Tarantelli, T.; Zanazzi, P. F. *Inorg. Chem.* **1982**, *21*, 1396. (f) Walker, J. D.; Poli, R. *Inorg. Chem.* **1990**, *29*, 756–761. (g) Bertrand, J. A.; Eller, P. G. *Inorg. Chem.* **1974**, *13*, 927. (h) Spartalian, K.; Bonadies, J.; Carrano, C. J. *Inorg. Chim. Acta* **1988**, *152*, 135–138. (i) Gerloch, M.; Mabbs, F. E. *J. Chem. Soc. A* **1967**, 1900. (j) Anderson, B. F.; Webb, J.; Buckingham, D. A.; Robertson, G. B. *J. Inorg. Biochem.* **1982**, *16*, 21–32. (k) Taft, K. L.; Lippard, S. J. *J. Am. Chem. Soc.* **1990**, *112*, 9629–9630. (l) Snyder, B. S.; Patterson, G. S.; Abrahamson, A. J.; Holm, R. H. *J. Am. Chem. Soc.* **1989**, *111*, 5214–5223.

Table IV. Relevant Structural Parameters for Dinuclear Oxoanion Complexes

complex	r(Fe–Fe) (Å)	r(M–X) (Å)	∠M–O–X	ref
	Terminal Monodentate Mode			
$[Fe_2(HPTB)\{O_2P(OPh)_2\}Cl_2(MeOH)]^{2+}$	3.70	3.35	147	51d
$[Mn^{IV}(HPO_4)bpy]_2(\mu\text{-}O)_2(\mu\text{-}PO_4)$		3.29	146	60
		3.36	160	
	Bridging Bidentate Mode (no μ-O(R) bridge)			
$[Fe(HDP)\{O_2P(OPh)_2\}]_2$	4.82	3.26	140	61
$[Fe_2(AsO_4)_3(Me_3TACN)_2]$	4.46	3.25	138	51a
		3.43	147	
		3.51	164	
	Bridging Bidentate Mode on an Fe(μ-OR)Fe Unit			
$[Fe^{III}_2O\{O_2P(OPh)_2\}_2\{HB(pz)_3\}_2]$	3.34	3.21	130	51b
$Fe^{II}Fe^{III}_2O(O_2PPh_2)_2\{HB(pz)_3\}_2]$	3.29	3.22	131	51b
$[Fe^{III}_2O\{O_3P(OPh)\}_2(Me_3TACN)_2]$	3.20	3.21	133	51a
$[Fe_2O\{O_2P(OPh)_2\}(TPA)_2]^{3+}$	3.36	3.17, 3.25	132	30
$[Fe^{II}Fe^{III}(BPMP)(O_2PPh_2)_2]^{2+}$	3.53	Fe^{III} 3.21 (3.15–3.27);	134	52
		Fe^{II} 3.29 (3.24–3.35)	132	
$[Fe^{III}Zn^{II}(BPMP)\{O_2P(OPh)_2\}_2]^{2+}$	3.70	Fe^{III} 3.18, 3.28	133, 141	51c
		Zn^{II} 3.21	131, 139	
$[Mn^{IV}(HPO_4)bpy]_2(\mu\text{-}O)_2(\mu\text{-}PO_4)$		3.06	126	60

of 3.06 Å would translate to an Fe–O–P angle of 121°, which is incompatible with the monodentate mode. Therefore, we conclude that the oxoanion most probably bridges the diferric site in the oxidized enzyme–oxoanion complexes.

The constraints imposed by the diiron core ($r_{Fe-\mu-O}$ = 1.95 Å and r_{Fe-Fe} = 3.2–3.3 Å) and the Fe–O–X angle of ~130° lead us to consider the two structures shown below for the diiron cores of Uf_o·PO_4 and Uf_o·AsO_4. $[Fe^{III}_2(OCH_3)(salen)(ehgs)]$ repre-

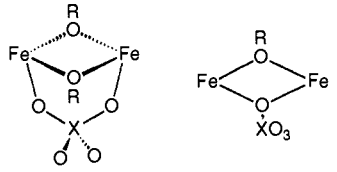

bidentate bridging XO_4 monodentate bridging XO_4

sents a complex with a (μ-methoxo)(μ-carboxylato-*O*)diiron(III) core,[59h] but there is no reported example of a complex with a monodentate oxoanion bridge. In addition, the geometrical constraints implicit for an Fe_2O_2 core structure (i.e., ∠Fe1–O–Fe2 + ∠Fe1–O–X + ∠Fe2–O–X ≤ 360°) argue against such a structure, especially for the arsenate complex. Given an Fe–O(As) distance of ~2.0 Å and an As–O distance of ~1.73 Å, an Fe–As distance of 3.41 Å requires an Fe–Fe distance of ≤3.0 Å; conversely, an Fe–Fe distance of 3.29 Å requires an Fe–As distance of 3.31 Å. Though the refined distances derived from the EXAFS analysis have associated errors, the distances needed to fit the monodentate bridging oxoanion model differ too much from the refined distances. We thus rule out this structure for Uf_o·PO_4 and Uf_o·AsO_4.

The alternative tribridged structure is exemplified by $[Fe_2(cat)_4(OAc)]^{3-}$,[59j] $[Fe(\mu\text{-}OMe)_2(\mu\text{-}O_2CCH_2Cl\text{-}O,O')]_{10}$,[59k] and $[Mn(HPO_4)bpy]_2(\mu\text{-}O)_2(\mu\text{-}PO_4\text{-}O,O')$.[60] The large number of synthetic complexes with bidentate bridging oxoanions suggests that oxoanions may favor the bidentate bridging coordination mode. Furthermore, the lengthening of the Fe–Fe distance on going from Uf_o·PO_4 to Uf_o·AsO_4 may reflect the response of the Fe_2O_2 core to the larger bite angle of a bidentate bridging arsenate. The effect of a supporting bridge on the M–M distance can be observed among synthetic complexes with bis(μ-OR)diiron(III)[46a,59] or bis(μ-oxo)dimanganese(IV) cores.[62] For $[Fe(OMe)_2(O_2CCH_2Cl)]_{10}$,[59k] the Fe–Fe distance is 0.1 Å shorter than those of other bis(μ-alkoxo)diiron(III) complexes having no supporting bridge, while for $[Mn(HPO_4)bpy]_2(\mu\text{-}O)_2(\mu\text{-}PO_4\text{-}O,O')$,[60] the Mn–Mn distance is at least 0.3 Å longer than those of other bis(μ-oxo)dimanganese(IV) complexes. We thus favor a $(\mu\text{-}OR)_2(\mu\text{-}XO_4\text{-}O,O')$diiron(III) core for Uf_o·PO_4 and Uf_o·AsO_4.

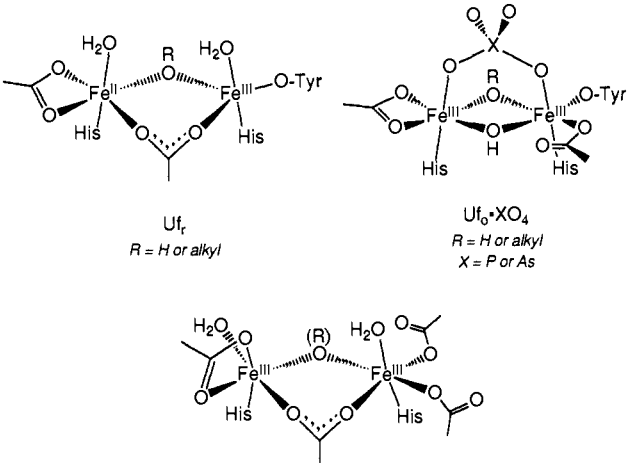

Figure 8. Proposed scheme for the diiron site of reduced uteroferrin and its oxidized anion complexes. For comparison are the diferric sites determined for the R2 protein of ribonucleotide reductase and proposed for the hydroxylase component of methane monooxygenase.

Summary and Perspective

The structural inferences we have drawn for the diiron site of uteroferrin from our EXAFS analysis of the native enzyme and its oxidized oxoanion complexes together with conclusions from previous spectroscopic studies are assembled in the scheme shown in Figure 8. The tyrosine and histidine ligands have been established previously on the basis of NMR studies,[17] while the presence of coordinated water is indicated by ESEEM[18] and electrochemical[19] studies. Several new features are suggested by the EXAFS results. Firstly, the shortest possible Fe–O distance for any of the uteroferrin complexes studied is ~1.93 Å, which is the expected length for Fe–phenolate and Fe–μ-hydroxo(or alkoxo) bonds[44–46] but much longer than expected for a μ-oxo bond. Therefore, this result and our preedge analyses exclude

(60) Sarneski, J. E.; Didiuk, M.; Thorp, H. H.; Crabtree, R. H.; Brudvig, G. W.; Faller, J. W.; Schulte, G. K. *Inorg. Chem.* **1991**, *30*, 2833–2835.
(61) Yan, S.; Que, L., Jr., unpublished observations.
(62) Thorp, H. H.; Brudvig, G. W. *New J. Chem.* **1991**, *15*, 479–490.

the presence of a μ-oxo bond in $Uf_o{\cdot}PO_4$ and $Uf_o{\cdot}AsO_4$. The absence of a Raman ν_s(FeOFe) feature[5] and the high redox potentials[19] associated with uteroferrin are also in agreement with the lack of an oxo bridge but are in conflict with magnetic susceptibility data indicating the absence of significant paramagnetism.[5,10,20]

Secondly, in all the first-sphere Uf data, there is an interference pattern at $k \approx 9$ Å^{-1} which is best modeled by a low Z atom at 2.4 Å. This scatterer is associated with a chelated carboxylate residue. Since the presence of a carboxylate coordinated to the Co site has been implicated by recent NOESY data on FeCoUf,[17c] we place this carboxylate on the redox-active iron center.

Thirdly, the 3.5-Å Fe–Fe distance associated with Uf_r suggests the presence of a (μ-OR)diiron core supported by a carboxylate bridge. Though there is presently no direct evidence for a bridging carboxylate, we believe that its involvement is very likely. Carboxylates are known to bridge metal–metal distances as large as 3.7 Å,[47d,63] and a bidentate bridging mode appears to be a very common binding motif.

The structure proposed for Uf_r thus shows a remarkable similarity to the diiron sites found for the R2 protein of the *E. coli* ribonucleotide reductase[13] and proposed for the hydroxylase component of methane monooxygenase (Figure 8).[64] All three structures have one His coordinated to each iron, a bidentate bridging carboxylate, and a chelated carboxylate on one iron. The terminal carboxylates on one iron in the RNR and MMO structures are replaced by tyrosine in the proposed Uf_r structure. These similarities may suggest the emergence of a common structural motif among a number of diiron–oxo proteins. However the ExxH sequences found in the primary structures of RNR R2 and MMO hydroxylase[64] are not found in purple acid phosphatases,[65] and the PAP His residues are respectively coordinated to the Fe(III) and the Fe(II) sites via N_ϵ and N_δ,[17b] in contrast to the RNR R2 His residues which are both N_δ-coordinated.[13]

Fourthly, phosphate and arsenate coordinate to the diiron unit of oxidized uteroferrin, consistent with electrochemical studies that show cathodic shifts in the uteroferrin redox potential upon anion binding.[19] The Fe–P and Fe–As distances found correspond to Fe–O–P(As) angles that are most consistent with bridging phosphate and arsenate. We suggest that the bridging carboxylate of Uf_r is converted into a terminal ligand to accommodate the oxoanion bridge in $Uf_o{\cdot}XO_4$. While there is no direct evidence for such a carboxylate shift,[66] a similar shift is observed for RNR R2, wherein one of the carboxylates of the bis(μ-carboxylato)diiron(II) core becomes a terminal ligand of the (μ-oxo)(μ-carboxylato)diiron(III) core.[67]

Lastly, despite their similar Fe–Fe distances, the core structure for $Uf_o{\cdot}PO_4$ and $Uf_o{\cdot}AsO_4$ must differ from the carboxylate-supported (μ-oxo)diferric cores of methemerythrin and ribonucleotide reductase, because of the absence of short Fe–μ-oxo bonds.[11,13,29,31] We propose an $Fe_2(\mu\text{-OR})(\mu\text{-OH})$ core structure supported by the bridging oxoanion. The new hydroxo bridge forms as a result of the Lewis acidity of the nascent Fe(III) center. This structure differs significantly from that proposed by Averill,[1c,5,25] who has favored a tribridged diferric core with bridging oxide, carboxylate, and oxoanion.

The diiron site of uteroferrin thus undergoes a significant change upon oxidation. At this point, it is not clear why the core structure changes upon oxidation nor why an oxo bridge does not form. We suggest the following for consideration: in diferric complexes, an oxo bridge usually forms between centers of moderate Lewis acidity; the corresponding bis(μ-hydroxo)diferric structure, a hydrated form of the μ-oxo species, may also form, but the equilibrium typically favors the μ-oxo species. The systematic study of dinuclear Fe^{III}(dipic) complexes by Hendrickson et al. illustrates this point; the parent ligand and its 4-OH and 4-$N(CH_3)_2$ derivatives afford bis(μ-hydroxo) complexes, while the 4-Cl derivative affords the μ-oxo complex.[68] Thus, one way to rationalize the $Uf_o{\cdot}XO_4$ results is to argue that the iron centers have sufficiently attenuated Lewis acidities as to favor the $Fe_2(OH)_2$ core. The presence of the doubly charged oxoanion and a tyrosine ligand (respectively replacing a bridging and a terminal carboxylate in the R2 structure, Figure 8) may favor such a structure.

Alternatively, a μ-oxo bridge would not form if the μ-OR group were an alkoxide, since dehydration of the $Fe_2(\mu\text{-OR})(\mu\text{-OH})$ core to form a $Fe_2(\mu\text{-O})$ moiety could not occur. The conditions for the formation of the decanuclear $[Fe(OMe)_2(OAc)]_{10}$ cluster are certainly basic enough for oxo bridge formation, but the presence of methoxide and not hydroxide affords the bis(μ-methoxo)(μ-acetato)diiron unit instead.[59k] Applying this argument to uteroferrin would make the μ-OR group in Uf_r an alkoxide (from one of a number of conserved Ser and Thr residues[65]), affording a (μ-alkoxo)(μ-carboxylato)diiron unit in Uf_r. Oxidation of the diiron unit in the presence of phosphate or arsenate generates an $Fe_2(\mu\text{-OH})(\mu\text{-OR})(\mu\text{-XO}_4)$ unit which cannot dehydrate to an $Fe_2(\mu\text{-O})$ core and converts the bridging carboxylate into a terminal ligand. The notion of an alkoxo bridge may also apply to methane monooxygenase, which is proposed to have a very similar ligand environment as RNR R2[16,55,64] but is not oxo-bridged in its diferric form.[55,69]

Acknowledgment. This research was supported at the University of Minnesota by National Science Foundation grant DMB-9104469 (L.Q.) and at Haverford College by the Undergraduate Biological Sciences Education Initiative of the Howard Hughes Medical Institute (R.C.S.). A.E.T. and R.C.H. are grateful for National Research Service Fellowships from the National Institutes of Health (GM-12792 and GM-13919, respectively), and C.R.R. acknowledges a traineeship from the National Institutes of Health (GM-07323). Beamline X9A at the NSLS at BNL is supported by the N.I.H. (RR-01633), while CHESS is supported by the N.S.F. (DMR-8412465). We would like to thank Drs. Michael J. Maroney and Gerald Kolpas from the University of Massachusetts, Dr. Syed Khalid from the National Biostructures PRT, and Drs. John B. Lynch, Timothy E. Elgren, and Richard E. Norman from the University of Minnesota for assistance in the data collection. We also thank Professor Karl S. Hagen for a sample of $[Fe(cyclen)OAc]CF_3SO_3$ and for sharing his structural results prior to publication.

(63) Holman, T. R.; Andersen, K. A.; Anderson, O. P.; Hendrich, M. P.; Juarez-Garcia, C.; Münck, E.; Que, L., Jr. *Angew. Chem., Int. Ed. Engl.* **1990**, *29*, 921–923.

(64) Nordlund, P.; Dalton, H.; Eklund, H. *FEBS Lett.* **1992**, *307*, 257–262.

(65) (a) Vincent, J. B.; Averill, B. A. *FEBS Lett.* **1990**, *263*, 265–268. (b) Ketcham, C. M.; Roberts, R. M.; Simmen, R. C. M.; Nick, H. S. *J. Biol. Chem.* **1989**, *264*, 557–563. (c) Ek-Rylander, B.; Bill, P.; Norgård, M.; Nilsson, S.; Andersson, G. *J. Biol. Chem.* **1991**, *266*, 24684–24689.

(66) Rardin, R. L.; Tolman, W. B.; Lippard, S. J. *New J. Chem.* **1991**, *15*, 417–430.

(67) Atta, M.; Nordlund, P.; Åberg, A.; Eklund, H.; Fontecave, M. *J. Biol. Chem.* **1992**, *267*, 20682–20688.

(68) (a) Ou, C. C.; Wollman, R. G.; Hendrickson, D. N.; Potenza, J. A.; Schugar, H. J. *J. Am. Chem. Soc.* **1978**, *100*, 4717–4724. (b) Ou, C. C.; Lalancette, R. A.; Potenza, J. A.; Schugar, H. J. *J. Am. Chem. Soc.* **1978**, *100*, 2053–2057.

(69) Fox, B. G.; Surerus, K. K.; Münck, E.; Lipscomb, J. D. *J. Biol. Chem.* **1988**, *263*, 10553–10556.